HfO_2 and SiO_2 as barriers in magnetic tunneling junctions

Gokaran Shukla, Thomas Archer, and Stefano Sanvito
School of Physics, AMBER and CRANN Institute, Trinity College, Dublin 2, Ireland
(Received 15 July 2016; revised manuscript received 14 January 2017; published 9 May 2017)

SiO_2 and HfO_2 are both high-k, wide-gap semiconductors, currently used in the microelectronic industry as gate barriers. Here we investigate whether the same materials can be employed to make magnetic tunnel junctions, which in principle can be amenable for integration in conventional Si technology. By using a combination of density functional theory and the nonequilibrium Green's functions method for quantum transport we have studied the transport properties of Co[0001]/SiO_2[001]/Co[0001] and Fe[001]/HfO_2[001]/Fe[001] junctions. In both cases we found a quite large magnetoresistance, which is explained through the analysis of the real band structure of the magnets and the complex one of the insulator. We find that there is no symmetry spin filtering for the Co-based junction since the high transmission $\Delta_{2'}$ band crosses the Fermi level, E_F, for both spin directions. However, the fact that Co is a strong ferromagnet makes the orbital contribution to the two $\Delta_{2'}$ spin subbands different, yielding magnetoresistance. In contrast for the Fe-based junction symmetry filtering is active for an energy window spanning between the Fermi level and 1 eV below E_F, with Δ_1 symmetry contributing to the transmission.

DOI: 10.1103/PhysRevB.95.184410

I. INTRODUCTION

The discovery by Fert [1] and Grünberg [2] of the giant magnetoresistance (GMR) effect in metallic magnetic multilayers is often considered as the kick off of the now-well-established field of *spintronics* [3]. GMR is the drastic change in the resistance of a magnetic nanostructure when its magnetic configuration is modified by a magnetic field. The simplest of such nanostructure is the spin valve, made of two magnetic layers separated by a nonmagnetic spacer. The two different magnetic configurations are obtained by aligning the magnetization vectors of the two magnetic layers either parallel (PA) or antiparallel (AP) to each other, with the parallel configuration often displaying the lower resistance. The same effect can be found when the spacer is an insulator and the charge carriers tunnel through its potential barrier. In this case the effect is called tunneling magnetoresistance (TMR) and the spin valve is a magnetic tunnel junction (MTJ).

The first evidence for TMR was provided in the seventies for a Fe/Ge/Co MTJ at low temperature by Jullière [4], who also established a simple formula to relate the magnitude of the effect to the spin polarization of the local density of states (DOS) of the two magnetic electrodes. Such spin polarization is simply defined as $p = \frac{D_\uparrow - D_\downarrow}{D_\uparrow + D_\downarrow}$, with D_σ being the DOS of the majority ($\sigma = \uparrow$) and minority ($\sigma = \downarrow$) electrons. Note that, depending on the particular experiments, the spin polarization of the current is not always proportional to that of the DOS [5]. A key result from Jullière's analysis is that, since the spin polarization of magnetic transition metals is of the order of 50%, relatively small TMRs have to be expected. If one uses the "optimistic" definition of TMR, TMR $= \frac{I^{PA} - I^{AP}}{I^{AP}}$, with I^{PA} (I^{AP}) being the current for the PA (AP) configuration, then Jullière's theory returns us TMRs no larger than 60–70%. Such prediction has been confirmed through the nineties with many experimental demonstrations of room temperature TMR in various MTJs, mostly using amorphous Al_2O_3 as insulating spacer [6,7].

A major breakthrough came in early 2000, when Butler [8] and Mathon [9] independently demonstrated that epitaxial MTJs could in practice sustain an arbitrarily large TMR. This is because in epitaxial junctions the transverse k vector (in the plane perpendicular to the MTJ stack direction), $\mathbf{k}_\parallel$, is conserved and the decay of the wave function of the tunneling electrons across the barrier depends on the orbital symmetry. For MgO along the [100] direction the states with the slowest decay rate are those around the Γ point in the transverse Brillouin zone with Δ_1 symmetry. In Fe such symmetry is present along the [100] direction near the Fermi level, E_F, only for the majority electrons. As such a [100]-oriented Fe/MgO structure will effectively behave as a half metal, if the barrier is thick enough. Such predictions were soon confirmed experimentally with reported room-temperature TMRs well exceeding 200% for the Fe/MgO/Fe system [10,11], and now [100]-oriented FeCoB/MgO/FeCoB structures are at the foundation of a multitude of applications, ranging from magnetic data storage to sensors [3].

Despite that the concept of orbital-spin filtering applies to several stacks, such as [100] $SrRuO_3/BaTiO_3$ and $SrRuO_3/SrTiO_3$ [12], [100] Cu/EuO [13], Co(0001)/h-BN [14], [100] Co_2MnSi/MgO [15], and a few others, the FeCoB/MgO system is at present the only one used in mainstream applications. There are several reasons behind this fact including the highly perfected growth technology for such a stack and the temperature robustness of the magnetic properties of the Fe-Co alloy. Yet, FeCoB/MgO presents also some disadvantages. For instance the Gilbert damping constant of Fe is large, so that applications based on spin-transfer torques are unlikely to be possible.

It is then important to enlarge the materials choice and thus design new possible stacks, not involving FeCoB and MgO. Here we investigate theoretically two of such possibilities and study in details MTJs constructed with either SiO_2 or HfO_2 as barrier and with either Fe or Co as electrodes. SiO_2 and HfO_2 are both wide-gap semiconductors and they are already widely used in the microelectronics industry as gate oxides, while *hcp* Co has a small damping constant [16]. It is then expected that such new junctions will be highly compatible with standard CMOS technology and may offer

the advantage of bringing memory elements close to the logic ones.

The paper is organized as follows. In the next section we present our computational method and the details of our calculations. Then we move on to describe our results by first looking at the intrinsic band structures of both the barriers and the electrodes and then by discussing the TMR. Finally we conclude.

II. COMPUTATIONAL DETAILS

We perform electronic structure and quantum transport calculations by using, respectively, density functional theory (DFT) and the nonequilibrium Green's functions method, still implemented with the Kohn-Sham DFT Hamiltonian (the NEGF+DFT scheme). The electronic structure of the various materials is calculated with the pseudopotential local-orbital basis set SIESTA code [17] in the local density approximation (LDA) [18]. When computing the complex band structure of SiO_2 and HfO_2 we use unit cells oriented, respectively, along the [0001] and the [001] directions, reflecting their hexagonal and cubic structure (for a discussion on the polymorphs of HfO_2 see Ref. [19]). In both cases we consider a grid spacing equivalent to a plane-wave cutoff of 700 Ryd and Monkhorst-Pack k-point meshes of $8 \times 8 \times 8$ and $5 \times 5 \times 5$, respectively, for HfO_2 and SiO_2. Note that the complex band structure is by definition always calculated along the z direction, so that there is no need to sample the $\mathbf{k} \parallel \hat{z}$ direction. Finally we have considered a double zeta basis set for the s, p, and d shells of Co and Fe, and s and p double zeta plus polarization orbitals for Si, Hf, and O.

We then construct two different MTJs, namely $Co/SiO_2/Co$ and $Fe/HfO_2/Fe$. In the first, both the electrodes and the barrier have a hexagonal structure, Co being in its natural occurring *hcp* lattice and SiO_2 in the α-quartz phase (space group $P3_221$). The experimental in-plane lattice constants are 2.51 Å for Co and 4.91 Å for SiO_2, so that for a stack grown along the [0001] direction the lattice mismatch is about 2%. The epitaxy is then achieved by placing the Co atoms facing the O ones at the interface. In contrast both the barrier and the electrodes in $Fe/HfO_2/Fe$ have cubic structure with experimental lattice constants of 5.08 Å and 2.82 Å, respectively, for HfO_2 and Fe. In this case the lattice mismatch is more significant, of the order of 10%, and again epitaxy is achieved by placing the Fe atoms on top of O at the interface. When constructing the MTJ stacks we fix the in-plane lattice constant to 4.91 Å for Co/SiO_2 and to 5.64 Å for Fe/HfO_2 and relax the atomic coordinates by conjugate gradient until the forces are smaller than 0.01 eV/Å. In particular, we consider two junctions where the SiO_2 and HfO_2 barriers are, respectively, 30.0 Å and 22.15 Å.

Note that in the case of Fe/HfO_2 the large lattice mismatch implies significant strain in the junction. Here we have taken as common in-plane lattice parameter for the $Fe/HfO_2/Fe$ MTJ the one of Fe, i.e., we have significantly expanded the lattice constant of HfO_2. We have verified that the HfO_2 band gap (as calculated with the LDA) does not change in a significant way over such range of lattice parameters. In fact, it varies in a nonmonotonic fashion when the lattice parameter goes from that of bulk HfO_2 (5.08 Å) to that chosen for the junction (5.64 Å), with the maximum variation being of the order of 0.4 eV. We then expect that our results will be rather insensitive (at least at a qualitative level) to the exact in-plane lattice parameter.

Transport calculations are performed with the SMEAGOL code [20–22], which implements the NEGF+DFT method with SIESTA as DFT platform. SMEAGOL calculates the electrical current at a given applied voltage, V, for spin σ ($\sigma = \uparrow, \downarrow$) from the Landauer-Büttiker formalism as

$$I^{\sigma}(V) = \frac{e}{h} \int dE\, T^{\sigma}(E;V)[f_{\mathrm{L}} - f_{\mathrm{R}}]\,, \tag{1}$$

where e is the electron charge, h the Plank constant, $T^{\sigma}(E;V)$ the energy- and voltage-dependent transmission coefficient, and f_{L} (f_{R}) the Fermi function associated with the left-hand- (right-hand-)side electrode. This is evaluated at $E - \mu_{\mathrm{L}}$ ($E - \mu_{\mathrm{R}}$), where $\mu_{\mathrm{L/R}} = E_{\mathrm{F}} \pm \frac{eV}{2}$ is the chemical potential for the left/right electrode. Since the junction is translationally invariant in a plane perpendicular to the transport direction the transmission coefficient can be written as

$$T^{\sigma}(E;V) = \frac{1}{\Omega_{\mathrm{BZ}}} \int_{\mathrm{BZ}} d\mathbf{k}_{\parallel}\, T^{\sigma}_{\mathbf{k}_{\parallel}}(E;V)\,, \tag{2}$$

where the sum extends over the two-dimensional Brillouin zone in the plane perpendicular to the transport direction and with area Ω_{BZ}. The transport calculations presented here are for the zero-bias limit only and are obtained by converging the charge density over a $8 \times 8 \times 1$ k-point grid and the transmission coefficient over a $50 \times 50 \times 1$ one. We have also performed additional tests for a $100 \times 100 \times 1$ mesh, without noting any significant change in $T^{\sigma}(E;V)$ or the TMR.

III. RESULTS AND DISCUSSION

A. SiO_2 and HfO_2 as tunneling barriers

SiO_2 and HfO_2 are both wide-gap insulators widely used as gate oxides in the fabrication of nanotransistors. For SiO_2 our LDA calculations return an indirect band gap of 5.6 eV with valence band maximum at the K point and the conduction band minimum at Γ. This, as expected, is smaller than the experimental one, which is about 9 eV. For cubic HfO_2 the LDA gives us a direct band gap at X of 3.7 eV, which also in this case is underestimated. In fact, although we could not find experimental measures for the cubic phase of HfO_2, the experimental range for the tetragonal one is 5–6 eV. Interestingly GW calculations report a gap value of 5.2 eV for the cubic phase and 6.1 eV for the tetragonal one [19], suggesting that the LDA underestimation of the experimental gap may be in the range of 2 eV. Note that we could have corrected the band gap in the transport calculations by, for instance, applying a self-interaction corrections method [23,24] or simply a scissor operator [25]. However, considering that the band gaps are already rather large we have decided to continue the calculations at the LDA level. It is expected that the gap corrections in this case will introduce only quantitative effects, leaving the general physics of the problem unchanged.

Next we move to evaluate how the wave function decays in the insulating barrier along the chosen directions. This is achieved by calculating the complex band structure of the two materials. For a periodic solid the energy dispersion is

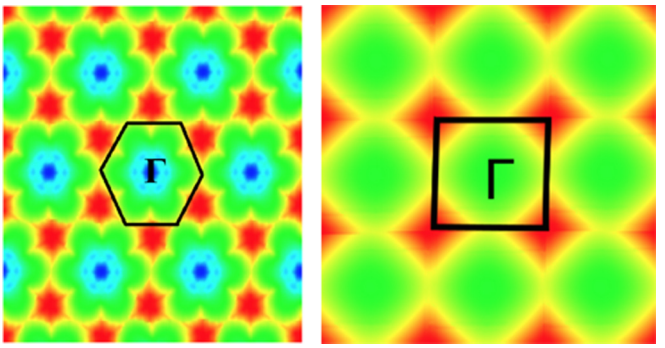

FIG. 1. Heat color plots of the wave-function decay coefficient, $\kappa(E_F,\mathbf{k}_\parallel)$, as a function of the transverse wave vector, $\mathbf{k}_\parallel$, for SiO_2 (left-hand-side panel) and HfO_2 (right-hand-side panel). Calculations are carried out for E_F placed in the middle of the band gap. The black boxes mark the 2D Brillouin zones and the color code is blue to green to red as κ gets larger. In both cases the decay coefficient is plotted in linear scale with the following limit: SiO_2 $\kappa_{min} = 3.16\,\text{Å}^{-1}$, $\kappa_{max} = 3.96\,\text{Å}^{-1}$; HfO_2 $\kappa_{min} = 1.33\,\text{Å}^{-1}$, $\kappa_{max} = 2.74\,\text{Å}^{-1}$.

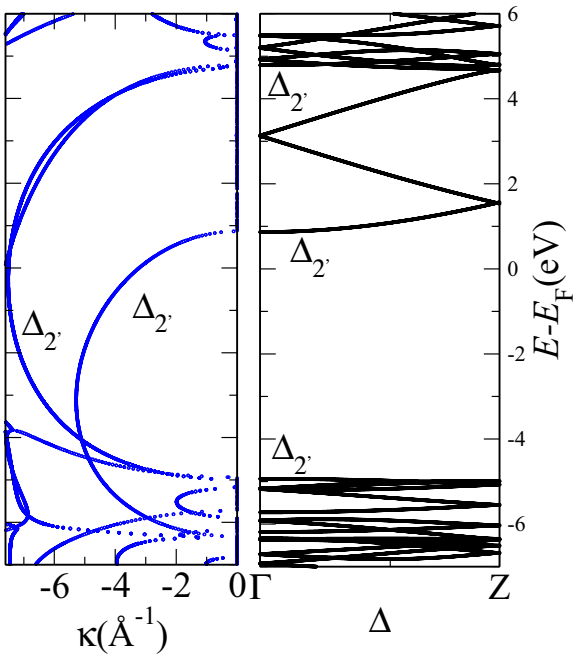

FIG. 2. Real (right-hand-side panel) and complex (left-hand-side panel) band structure of SiO_2 calculated at the Γ point in the 2D transverse Brillouin zone. The symmetry labels, Δ_n, have been described in the text and the Fermi energy is taken in the middle of the gap.

obtained by calculating the N possible eigenvalues $\epsilon_n(k_x,k_y,k_z)$ corresponding to the real k vector $\mathbf{k} = (k_x,k_y,k_z)$, where N is the number of basis functions in the unit cell. One can also solve the inverse problem and find the k_z component of the wave vector (z is the direction of interest, namely the one of the transport), once both the transverse $\mathbf{k}_\parallel = (k_x,k_y)$ component and the energy E are fixed. When E corresponds to the material energy gap (or to minigaps) then the equation $E = \epsilon(\mathbf{k}_\parallel,k_z)$ can be solved for complex $k_z = q + i\kappa$. The transmission coefficient is expected to decay as a function of the barrier thickness d, as $T(E,\mathbf{k}_\parallel) \sim T_0(E,\mathbf{k}_\parallel)e^{-2\kappa(E,\mathbf{k}_\parallel)d}$, where $T_0(E,\mathbf{k}_\parallel)$ in general depends on the nature of the interface between the metal and the insulator. One can then plot $\kappa(E_F,\mathbf{k}_\parallel)$ across the 2D Brillouin zone spanned by the transverse wave vector $\mathbf{k}_\parallel$ and establish which portions of the Brillouin zone contribute the most to the tunneling current. The results of such an exercise are presented in Fig. 1.

From the figure is it clear that for both insulators the minimum decay coefficient is found in the middle of the 2D Brillouin zone, namely at the Γ point. This corresponds to tunneling electrons having wave vectors parallel to the transport direction, i.e., electrons that approach the energy barrier perpendicularly to the interface between the metal and the insulator. A situation as the one presented here is most typical, and it is encountered for featureless potential barriers and parabolic band dispersions (the Fermi surface is spherical). It is also the same situation found for MgO along the [001] direction. One should also note that, in general, the decay across SiO_2 is significantly faster than that across HfO_2, owing to its larger band gap. Such decay coefficients are expected to become larger as the band gap increases, so that corrections to the band gap magnitude will change the rate of decay. These, however, will not modify the distribution of $\kappa(E_F,\mathbf{k}_\parallel)$ across the Brillouin zone.

Next we need to analyze how the complex band structure of the insulators relate to the real one of the magnetic electrodes. The tunneling process in epitaxial junctions preserves the transverse wave vector and only states with the same $\mathbf{k}_\parallel$ and the same symmetry contribute to the current. As such we now analyze the symmetry of the real and complex band structure of the insulator along the direction of the transport at $\mathbf{k}_\parallel = \Gamma$, namely in the region of the 2D Brillouin zone, where the wave function decay is minimum. Note, however, that this analysis provides only a tool for interpreting the behavior of the transmission coefficient as a function of energy in terms of the band structure. The transmission itself, as explained in the Method section, is evaluated by integrating over the entire $\mathbf{k}_\parallel$ Brillouin zone and not by taking its value at the Γ point only.

The symmetry of the Bloch states can be assigned by looking at their atomic orbital composition. In particular we denote as Δ_1 a Bloch state made of orbitals having zero angular momentum with respect to an axis orthogonal to the interface with the metal, namely s, p_z, and $d_{3z^2-r^2}$ orbitals. In contrast, we label as Δ_2 orbitals with $d_{x^2-y^2}$ character and as $\Delta_{2'}$ those with a d_{xy} one. Finally the Δ_5 symmetry is assigned to p_x, p_y, d_{xz}, and d_{yz} orbitals. The real and complex band structure for SiO_2 and HfO_2 calculated at the Γ point in the 2D transverse Brillouin zone are presented in Figs. 2 and 3, respectively.

In general the complex bands appear smooth and connect the edges of the conduction and the valence band across the gap. We do not detect any sign of the spurious flat complex bands, which sometimes appear when one considers nonorthogonal local-orbital basis sets, and in general they agree well with results available in literature [26].

The two insulators display a rather different behavior. In fact, SiO_2 has a complex band structure entirely dominated by the $\Delta_{2'}$ symmetry. The band presenting the slowest decay rates originates from one of the valence bands about 1 eV below the valence band maximum and closes at the conduction band

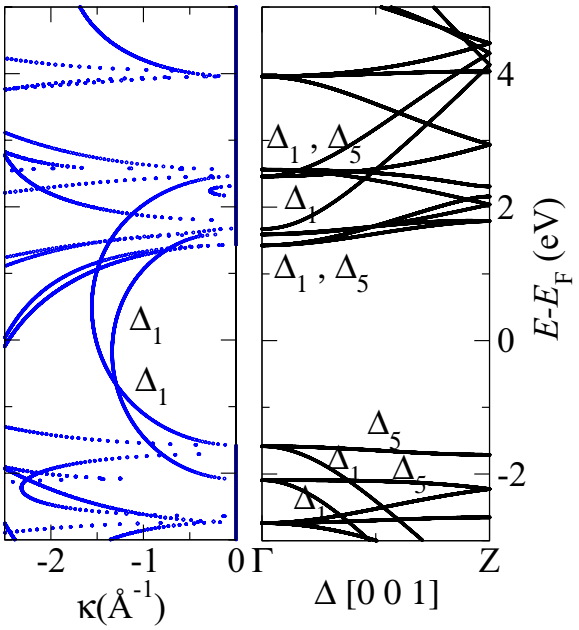

FIG. 3. Real (right-hand-side panel) and complex (left-hand-side panel) band structure of HfO_2 calculated at the Γ point in the 2D transverse Brillouin zone. The symmetry labels, Δ_n, have been described in the text and the Fermi energy is taken in the middle of the gap. Note that the two complex bands crossing the gap present Δ_1 symmetry, while there are also bands with much larger κ and Δ_5 symmetry.

minimum. There are two other complex bands at the valence band maximum, also with $\Delta_{2'}$ symmetry, which however have a rather large curvature. As such these provide the slowest decay rate only in a tiny energy window around the top of the valence band and will not contribute to the transport, unless the Fermi level of the junction is pinned close to the valence band. In contrast HfO_2 has a band gap dominated by two intersecting complex bands presenting Δ_1 symmetry (as identified from the orbital projections). These have a similar curvature and they appear shifted by about 1 eV with respect to each other.

B. Symmetry of the magnetic electrodes

We now move to analyze the symmetry of the real band structure of the magnetic electrodes along the direction of the transport. The most favorable situation is that in which one of the two spin subbands presents Bloch states at the Fermi energy with the same symmetry of those in the complex band of the insulator, while the other spin subband does not. In this case only one spin direction will be transmitted with high efficiency and the electron/insulator stack will effectively behave as a half metal with the magnetoresistance increasing exponentially with the barrier thickness. For instance, this is the situation encountered for Fe/MgO along the [001] direction [8,9].

The real band structure of hcp Co along the [0001] direction and of bcc Fe along the [001] one are plotted in Figs. 4 and 5, respectively.

We find that both magnetic electrodes supply Bloch states with the symmetry required by the insulator for each of the

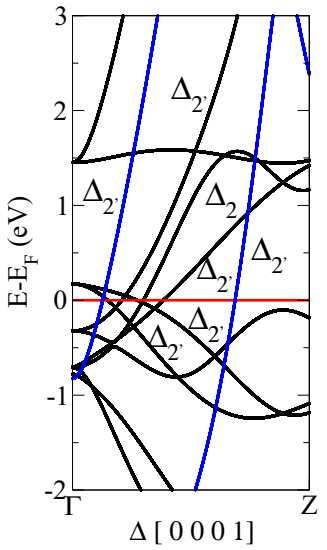

FIG. 4. Real band structure of hcp Co plotted along the [0001] transport direction. The majority spin subband is in blue and the minority one in black.

two spin directions. In the case of hcp Co there are bands with $\Delta_{2'}$ symmetry crossing the Fermi energy for both majority and minority spins. These are shifted with respect to each other by the exchange energy, but unfortunately provide high transmission for both spins. However, since Co is a strong ferromagnet with fully filled majority d band, the majority $\Delta_{2'}$ band at E_F has to be attributed to hybrid spd states, so that the d orbital content is expected to be different from that of its minority counterpart.

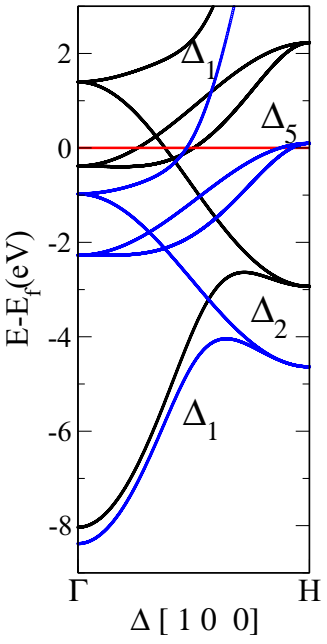

FIG. 5. Real band structure of bcc Fe plotted along the [001] transport direction. The majority spin subband is in blue and the minority one in black.

The case of bcc Fe along [001] is different. In fact, there is only one majority band with Δ_1 symmetry at E_F, while there are also Δ_5 states for both spins. In particular the Fermi level crosses the top of the majority Δ_5 band and the bottom of the minority one. Thus, we expect single spin filtering for the majority Δ_1 channel and some residual transmission for Δ_5 electrons with both spin directions.

C. Tunnel magnetoresistance

We finally turn our attention to the TMR of the proposed junctions and we start our analysis from the $Co/SiO_2/Co$ one. The transmission coefficient as a function of energy is plotted for both spin channels and for both the parallel and antiparallel configurations in Fig. 6. As expected, in general, $T(E)$ drops drastically in an energy region approximately 6 eV wide, which corresponds to the calculated SiO_2 band gap (along the transport direction). The Fermi level of the junction is positioned about 2 eV above the SiO_2 valence band so that the MTJ at low bias is deep in the tunneling regime. Furthermore, once $T(E)$ is plotted in logarithmic scale as in Fig. 6, one can notice that $\log[T(E)]$ as a function of E effectively follows the lower-lining complex band structure of SiO_2. This confirms that the transport is essentially dominated by the $\Delta_{2'}$ states identified by our symmetry analysis.

If one now focuses the attention on $T^\sigma(E)$ for the two spins in the parallel configuration, it is easy to note that there are

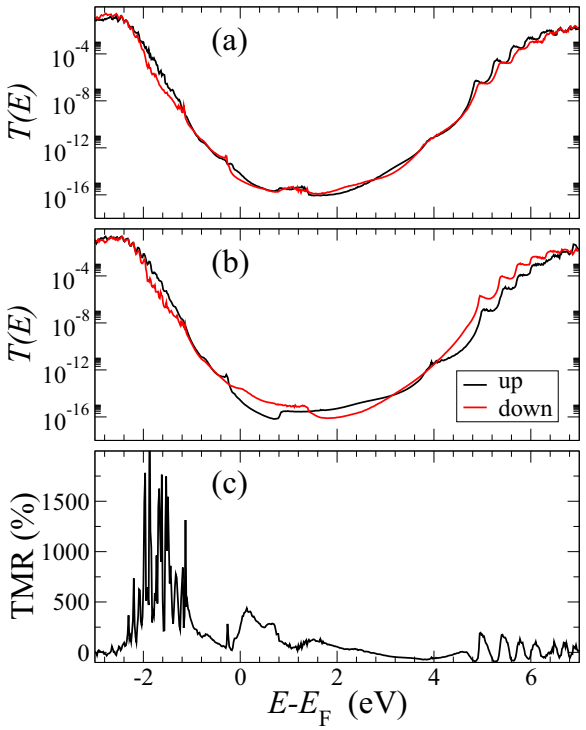

FIG. 6. Transmission coefficient as a function of energy for the $Co/SiO_2/Co$ MTJ. The parallel and antiparallel configurations are plotted in panel (a) and (b), respectively. $T(E)$ for the majority (minority) spins is plotted in black (red). For the antiparallel case the spin direction is set by the left-hand-side electrode. The transmission coefficient is plotted in logarithmic scale. In the lower panel (c) we present the calculated zero-bias TMR as a function of energy in the same energy window of the transmission coefficients.

two energy regions where the transmission is dominated by one spin. This happens between E_F and $E_F + 1$ eV for the minority spin and between 1.5 eV and 3 eV above E_F for the majority one. It is difficult to ascribe such dependence to some clear features of the band structure along the transport direction since there are several bands with the right symmetry and, in addition, the transmission coefficient is integrated over the entire Brillouin zone, so that an entire region of k points around Γ contributes to the transport. The same situation is not encountered for the antiparallel configuration for which the $T^\sigma(E)$'s are almost spin degenerate, since a majority (minority) electron in one electrode travels in the minority (majority) band of the other electrode. As such the transmission coefficient for the antiparallel configuration is approximately a convolution of the transmission coefficients for the two spins in the parallel configuration. Note that here the spin degeneracy in the AP configuration is not exact since the two Co/SiO_2 surfaces relaxed to a slightly different geometry, so that the junction does not possess inversion symmetry.

The resulting TMR as a function of energy is plotted in the lower panel of Fig. 6 for an energy window of 2 eV around E_F. As expected from our analysis of the transmission coefficients we find a significant TMR in a region 1 eV wide above the Fermi level. The maximum value of about 450% is reached at $E = E_F + 0.14$ eV, while the calculated TMR at the Fermi energy is approximately 250%. This is indeed larger than what we expected from the simple density of state argument brought by Jullière's analysis, indicating that some spin filtering effect is at play. However, our discussion on the band structure of the insulator and the electrodes suggests that, if such spin filtering takes place, it will be related either to complex bands with $\Delta_{2'}$ symmetry and large decay constant, or to portions of the 2D Brillouin zone away from the Γ point.

Finally we take a look at the $Fe/HfO_2/Fe$ MTJ. In this case the various transmission coefficients are shown in Fig. 7, again plotted in logarithmic scale. In this case the situation is significantly more complex since the $T(E)$'s present quite some structure even in the gap region. The band gap is about 4 eV and the Fermi level cuts approximately 1 eV above the valence band maximum. Let us start the discussion once again from the majority spins in the parallel configuration.

In this case $T(E)$ displays relatively high transmission in the energy region comprised between $E_F - 1$ eV and E_F, a region corresponding to the presence of bands with both Δ_1 and Δ_5 symmetry. For $E > E_F$ the transmission drops significantly, although the Δ_1 band is still present and it is the low-transmission Δ_5 symmetry to stop contributing.

When the same analysis is carried out on the minority spin band we find a region of small transmission between $E_F - 1$ eV and E_F. This is a region where there is no either Δ_1 or Δ_5 bands, since the first of the Δ_5 bands has its onset just around E_F. As one passes E_F the Δ_5 band starts to dominate the transport. This remains relatively large until one reaches the energy corresponding to the minority Δ_1 band, which is also the energy corresponding to the upper band edge of the Δ_5. This analysis clearly demonstrates that for $Fe/HfO_2/Fe$ there is some level of spin filtering, since in an energy region extending 1 eV below the Fermi level and terminating just above E_F the high transmission Δ_1 band appears only for majority spins.

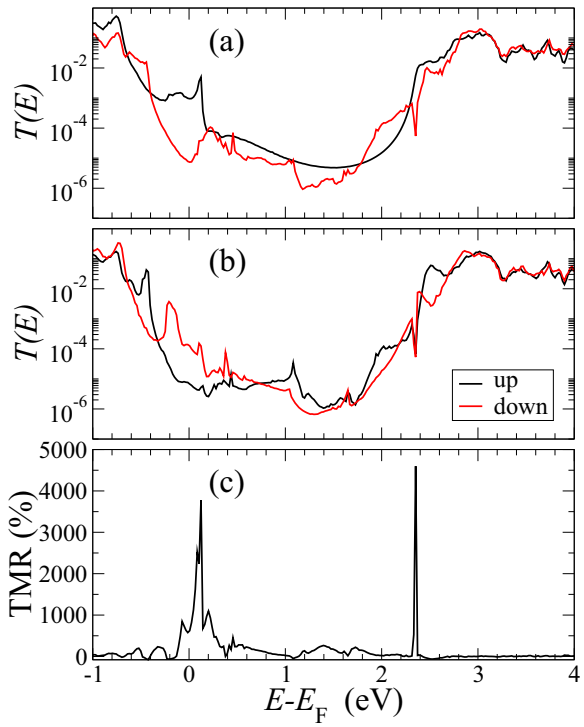

FIG. 7. Transmission coefficient as a function of energy for the $Fe/HfO_2/Fe$ MTJ. The parallel and antiparallel configurations are plotted in panel (a) and (b), respectively. $T(E)$ for the majority (minority) spins is plotted in black (red). For the antiparallel case the spin direction is set by the left-hand-side electrode. The transmission coefficient is plotted in logarithmic scale. In the lower panel (c) we present the calculated zero-bias TMR as a function of energy in the same energy window of the transmission coefficients.

As in the case of $Co/SiO_2/Co$ the transmission coefficients for the antiparallel configuration appear as some convolution of those for the two spins in the parallel one. However, since the band gap of HfO_2 is significantly smaller than that of SiO_2 and so is the complex component of the wave vector in the gap, the small differences between the left-hand and right-hand interfaces with the electrodes significantly lift the spin degeneracy of $T(E)$. Note that the analysis of the various transmission functions in terms of the complex band structure done here is not as sharp and definitive as the one that one can carry out for Fe/MgO. The reason behind such behavior is that indeed the transmission is maximized at Γ (see Fig. 1), but the complex wave vector at the Fermi level is a relatively smooth function across a wide region in the middle of the Brillouin zone. This means that a significant portion of the central part of the Brillouin zone may also contribute to the transport.

The TMR as a function of energy is then plotted in the lower panel of Fig. 7 and nicely corroborates our analysis. In fact we find a robust TMR, reaching up to 3500% for energies up to 0.25 eV above the Fermi level. This is the energy window where the tunneling in the majority subband is dominated by states with Δ_1 symmetry and that in the minority one by states with Δ_5. Note that the upper edge of the majority Δ_5 band almost coincides with the lower edge of the minority one, and the TMR is maximized essentially at that particular energy. At the calculated Fermi level the TMR is about 600%, which is significantly larger than that predicted by the Jullière's formula. In this case we can indeed identify the spin filtering mechanism at the Γ point as the main contributor to such large TMR, and therefore the $Fe/HfO_2/Fe$ MTJ can represent a valid alternative to other spin filtering MTJ stacks. Unfortunately, however, since the spin filtering occurs only in a relatively small energy window, we expect that the bias dependence of the TMR will be rather severe and that little TMR will be detected for biases larger than approximately 0.5 V.

IV. CONCLUSION

In summary, we have explored the possibility of using the wide-gap insulators SiO_2 and HfO_2 as tunnel barriers in novel magnetic tunnel junctions. Both SiO_2 and HfO_2 are currently used in the microelectronic industry so that MTJs based on such insulators have the potential to be integrated in hybrid memory/logic components. We have performed a complex band structure analysis and identified the dominant symmetry of the tunneling electrons in the two materials. We have found that electron transmission is high for Bloch states with $\Delta_{2'}$ symmetry in SiO_2, while it the Δ_1 to characterize HfO_2.

We have then investigated two possible MTJs, namely $Co/SiO_2/Co$ and $Fe/HfO_2/Fe$, respectively, oriented along the [0001] and the [001] direction. The first one does not present spin filtering for any energies around E_F since Co supplies electrons with $\Delta_{2'}$ for both spins. However, since Co is a strong magnet the orbital character of such $\Delta_{2'}$ band appears different for the two spins and still a significant zero-bias TMR is found. In contrast, the $Fe/HfO_2/Fe$ MTJ presents spin filtering and the TMR is predicted rather large for a relative narrow energy just above E_F. Our work has demonstrated that SiO_2 and HfO_2 can be used as tunnel barriers in MTJs, although for high performance junctions one probably has to look at magnetic electrodes different from simple transition metals.

ACKNOWLEDGMENTS

This work is supported by Science Foundation Ireland (Grant No. 14/IA/2624 and AMBER Center). We also gratefully acknowledge the DJEI/DES/SFI/HEA Irish Centre for High-End Computing (ICHEC) for the provision of computational facilities and support and the Trinity Centre for High Performance Computing (TCHPC) for technical support.

[1] M. N. Baibich, J. M. Broto, A. Fert, F. N. Van Dau, F. Petroff, P. Etienne, G. Creuzet, A. Friederich, and J. Chazelas, Phys. Rev. Lett **61**, 2472 (1988).

[2] G. Binasch, P. Grünberg, F. Saurenbach, and W. Zinn, Phys. Rev. B **39**, 4828 (1989).

[3] *Handbook of Spin Transport and Magnetism*, edited by E. Y. Tsymbal and I. Zutic (Chapman and Hall/CRC, 2011).

[4] M. Jullière, Phys. Lett. A **54**, 225 (1975).

[5] I. I. Mazin, Phys. Rev. Lett. **83**, 1427 (1999).

[6] T. Miyazaki and N. Tezuka, J. Magn. Magn. Matter. **139**, L231 (1995).
[7] J. S. Moodera, L. R. Kinder, T. M. Wong, and R. Meservey, Phys. Rev. Lett. **74**, 3273 (1995).
[8] W. H. Butler, X.-G. Zhang, T. C. Schulthess, and J. M. MacLaren, Phys. Rev. B **63**, 054416 (2001).
[9] J. Mathon and A. Umerski, Phys. Rev. B **63**, 220403 (2001).
[10] S. S. P. Parkin, C. Kaiser, A. Panchula, P. M. Rice, B. Hughes, M. Samant, and S. H. Yang, Nat. Mater. **3**, 862 (2004).
[11] S. Yuasa, T. Nagahama, A. Fukushima, Y. Suzuki, and K. Ando, Nat. Mater. **3**, 868 (2004).
[12] N. M. Caffrey, T. Archer, I. Rungger, and S. Sanvito, Phys. Rev. Lett. **109**, 226803 (2012).
[13] N. Jutong, I. Rungger, C. Schuster, U. Eckern, S. Sanvito, and U. Schwingenschlögl, Phys. Rev. B **86**, 205310 (2012).
[14] S. V. Faleev, S. S. P. Parkin, and O. N. Mryasov, Phys. Rev. B **92**, 235118 (2015).
[15] H. X. Liu, Y. Honda, T. Taira, K. I. Matsuda, M. Arita, T. Uemura, and M. Yamamoto, Appl. Phys. Lett. **101**, 132418 (2012).
[16] S. M. Bhagat and P. Lubitz, Phys. Rev. B **10**, 179 (1974).
[17] J. M. Soler, E. Artacho, J. D. Gale, A. Garcia, J. Junquera, P. Ordejón, and D. Sánchez-Portal, J. Phys.: Condens. Matter **14**, 2745 (2002).
[18] D. M. Ceperley and B. J. Alder, Phys. Rev. Lett **45**, 566 (1980).
[19] H. Jiang, R. I. Gomez-Abal, P. Rinke, and M. Scheffler, Phys. Rev. B **81**, 085119 (2010).
[20] A. R. Rocha, V. M. Garcia-Suarez, S. Bailey, C. J. Lambert, J. Ferrer, and S. Sanvito, Nat. Mater. **4**, 335 (2005).
[21] A. R. Rocha, V. M. García Suárez, S. Bailey, C. Lambert, J. Ferrer, and S. Sanvito, Phys. Rev. B **73**, 085414 (2006).
[22] I. Rungger and S. Sanvito, Phys. Rev. B **78**, 035407 (2008).
[23] C. D. Pemmaraju, T. Archer, D. Sánchez-Portal, and S. Sanvito, Phys. Rev. B **75**, 045101 (2007).
[24] A. Filippetti, C. D. Pemmaraju, S. Sanvito, P. Delugas, D. Puggioni, and V. Fiorentini, Phys. Rev. B **84**, 195127 (2011).
[25] A. M. Souza, I. Rungger, U. Schwingenschlögl, and S. Sanvito, Nanoscale **7**, 19231 (2015).
[26] F. Sacconi, J. M. Jancu, M. Povolotskyi and A. Di Carlo, IEEE Trans. El. Dev. **54**, 3168 (2007).